Journal of Biomolecular NMR **28:** 369–384, 2004.
KLUWER/ESCOM

Temperature-dependent spectral density analysis applied to monitoring backbone dynamics of major urinary protein-I complexed with the pheromone 2-*sec*-butyl-4,5-dihydrothiazole*

Hana Křížová[a], Lukáš Žídek[a,**], Martin J. Stone[b], Milos V. Novotny[c] & Vladimír Sklenář[a]
[a]*National Centre for Biomolecular Research, Faculty of Science, Masaryk University, Kotlářská 2, 61137 Brno, Czech Republic;* [b]*Department of Chemistry, Indiana University, Bloomington, IN 47405, U.S.A.;* [c]*Institute of Pheromone Research and Department of Chemistry, Indiana University, Bloomington, IN 47405, U.S.A.*

Received 9 September 2003; Accepted 29 October 2003

Key words: backbone dynamics, NMR relaxation, spectral density function, temperature dependence

Abstract

Backbone dynamics of mouse major urinary protein I (MUP-I) was studied by ^{15}N NMR relaxation. Data were collected at multiple temperatures for a complex of MUP-I with its natural pheromonal ligand, 2-*sec*-4,5-dihydrothiazole, and for the free protein. The measured relaxation rates were analyzed using the reduced spectral density mapping. Graphical analysis of the spectral density values provided an unbiased qualitative picture of the internal motions. Varying temperature greatly increased the range of analyzed spectral density values and therefore improved reliability of the analysis. Quantitative parameters describing the dynamics on picosecond to nanosecond time scale were obtained using a novel method of simultaneous data fitting at multiple temperatures. Both methods showed that the backbone flexibility on the fast time scale is slightly increased upon pheromone binding, in accordance with the previously reported results. Zero-frequency spectral density values revealed conformational changes on the microsecond to millisecond time scale. Measurements at different temperatures allowed to monitor temperature depencence of the motional parameters.

Introduction

Binding of mouse pheromones to major urinary proteins (MUPs) represents a typical example of interactions between lipocalins and their small hydrophobic ligands (Flower, 1996). Although the biological role of the variety of MUPs is still a matter of investigation (Beynon et al., 2002; Hurst et al., 2001; Marie et al., 2001; Novotny et al., 1999), structure of these proteins and of their complexes with ligands has been studied by NMR and X-ray crystallography (Böcskei et al., 1992; Žídek et al., 1999b; Lücke et al., 1999; Timm et al., 2001; Kuser et al., 2001). Binding of various pheromones and pheromone analogs to several MUP isoforms has been also studied by isothermal titrational calorimetry (Sharrow et al., 2002). In our previous study (Žídek et al., 1999a), we observed that the backbone flexibility of MUP isoform I (MUP-I) increased slightly upon pheromone binding, in contrast to the decreased flexibility expected for induced-fit interactions (Stone, 2001). Such an increase in flexibility may entropically favor the process of ligand binding. On the other hand, results of isothermal titrational calorimetry showed that the pheromone binding to MUPs is enthalpy-driven ($\Delta H = 46.9 \pm 0.4$ kJ mol^{-1} at 25 °C) and accompanied by a decrease in total entropy ($\Delta S = 39 \pm 2$ kJ mol^{-1}K^{-1} 25 °C and $-T\Delta S = 11.7 \pm 0.4$ kJ mol^{-1} at 25 °C) (Sharrow et al., 2003). As the dynamics of the protein backbone plays an important role in the protein-ligand interac-

*This work was supported by Grant No. 203/00/0511 from Grant Agency of the Czech Republic, Grant DC 02418 from the National Institute of Deafness and Communication Disorders, and by Grants MCB-9600968 and MCB-0212746 from the National Science Foundation.
**To whom correspondence should be addressed. E-mail: kriza@chemi.muni.cz

tions, we decided to investigate the backbone motions in more detail.

NMR relaxation of ^{15}N of the peptide bond provides the most popular probe of the protein backbone dynamics on a time-scale ranging from picoseconds to milliseconds. Currently, there are two commonly used methods of analyzing the relaxation data, model-free analysis (Lipari and Szabo, 1982a, b; Clore et al., 1990) and reduced spectral density mapping (Farrow et al., 1995a; Peng and Wagner, 1995; Ishima and Nagayama, 1995; Lefèvre et al., 1996). Model-free analysis is attractive because its results are expressed as quantities directly related to the spatial restriction and time-scale of the molecular motions. However, deciding which parameters should be fitted represents a difficult statistical task and may lead to false description of the motions (Schurr et al., 1994; d'Auvergne and Gooley, 2003; Idiyatullin et al., 2003).

Regardless of the method of analysis, limiting the experimental data to the three common parameters – the ^{15}N R_1 and R_2 and the heteronuclear $\{^1\mathrm{H}\}^{15}$N NOE – restricts the number of independent dynamics parameters available by data fitting. It is therefore advisable to extend the variability of data by changing the external conditions. One possibility is to acquire spectra at several magnetic fields, taking advantage of the field dependence of the relaxation (Peng and Wagner, 1995). Another possibility is to repeat the measurements at various temperatures. There are numerous examples of temperature-dependent studies of NMR relaxation in literature (for example, see Mandel et al., 1996; Landry et al., 1997; Bracken et al., 1999; Evenäs et al., 1999; Bertini et al., 2000; Spyracopoulos et al., 2001; Ramboarina et al., 2002).

As the dependence of relaxation parameters on the magnetic field is well understood, the use of several field strengths is very useful and convenient for data interpretation. The temperature dependence of molecular motions cannot be described so easily, but measuring relaxation parameters at various temperatures is attractive for several reasons. First, temperature dependence of motional parameters provides new insight into the protein dynamics, second, monitoring temperature changes does not require access to several expensive spectrometers, and third, all data can be acquired using the same spectrometer and probe, reducing the problem of compatibility.

In this article, we present relaxation data collected for both the free and pheromone-bound forms of MUP-I over a range of temperatures at 14.1 and 11.75 T. The data at each temperature are analyzed according to the reduced spectral density approach. In addition, we introduce fitting the multiple-temperature data to mathematical models that resemble the Lipari–Szabo formalism but which also incorporate the temperature-dependence of the usual model-free parameters. We discuss dynamical differences between the free and pheromone-bound forms of MUP-I.

Materials and methods

Recombinant MUP-I and 2-*sec*-butyl-4,5-dihydrothiazole were prepared as described elsewhere (Žídek et al., 1999b; Novotny et al., 1995). Samples of 1.8 mM uniformly ^{15}N-labeled MUP-I in 50 mM sodium phosphate buffer, pH 6.3 (uncorrected reading), containing 7.7% ^2H_2O were used in the presence or absence of twofold molar ratio of 2-*sec*-butyl-4,5-dihydrothiazole. The ^{15}N relaxation data were acquired on Bruker Avance 600 MHz and 500 MHz instruments equipped with 5-mm, z-gradient, triple resonance TXI probes. Standard T_1, T_2, and NOE experiments (Farrow et al., 1994) were run with the following relaxation delays: T_1, 11, 55, 133, 233, 377, 555, 888 and 1332 ms; T_2, 17, 33, 67, 100, 150, 200 and 238 ms. The last two T_2 time points were replaced with 118 and 178 ms for the two lowest temperatures at 14.1 T. The overall delay in NOE experiments was 9 s. The delay in the CPMG pulse train was set to 0.45 ms. Software NMRPipe (Delaglio et al., 1995) was used for spectra processing and exponential fitting.

Values of the reduced spectral density function were calculated from Equation 1 (Lefèvre et al., 1996):

$$\begin{pmatrix} J(0) \\ J(\omega_N) \\ J(0.87\omega_H) \end{pmatrix} = \begin{pmatrix} \frac{-3}{4(3d^2+c^2)} & \frac{3}{2(3d^2+c^2)} & \frac{-9}{10(3d^2+c^2)} \\ \frac{1}{(3d^2+c^2)} & 0 & \frac{-7}{5(3d^2+c^2)} \\ 0 & 0 & \frac{1}{5d^2} \end{pmatrix} \cdot \begin{pmatrix} \frac{1}{T_1} \\ \frac{1}{T_2} \\ \frac{\gamma_N}{\gamma_H}\frac{\mathrm{NOE}-1}{T_1} \end{pmatrix}, \quad (1)$$

where $d^2 = (\mu_0 h\gamma_N\gamma_H)^2/(16\pi^4 r^6)$ and $c^2 = \omega_N^2\Delta\sigma^2/3$. Values of amide bond length $r = 0.102$ nm, ^{15}N chemical shift anisotropy $\Delta\sigma = -160$ ppm, and ^{15}N angular velocity $\omega_N = 3.82 \times 10^{-8}$ rad s^{-1} (at 14.1 T) or 3.185×10^{-8} rad s^{-1} (at 11.75 T) were used in this study. The program GNUPLOT (T. Williams and C. Kelley) was utilized for graphical analysis of the results and nonlinear fitting to theoretical models.

Changes of spatial restriction upon the ligand binding were qualitatively identified in the following manner. First, the $J(\omega_N)$ vs. $J(0)$ correlations were plotted for all temperatures for individual residues of pheromone-bound and free MUP-I. Second, the temperature dependences of the plotted points was approximated with curves b (pheromone-bound) and f (free). Third, the rigidity change index (RCI) was defined as $B/B_t + F/F_t - 1$, where B is the number of data points of pheromone-bound MUP-I above curve f, F is the number of data points of free MUP-I below curve b, and B_t, F_t are the total number of data points available for the residue.

The model-free parameters were obtained by fitting the reduced spectral density function values to equations derived from the following general model (Ishima and Nagayama, 1995; Mandel et al., 1996):

$$J(0) = \frac{2}{5}a_0\tau_0 + \frac{2}{5}(1-a_0)\tau_1 + e^{A_{ex}+\frac{E_{ex}}{RT}}, \quad (2)$$

$$J(\omega_N) = \frac{2}{5}a_0\frac{\tau_0}{1+(\omega_N\tau_0)^2} + \frac{2}{5}(1-a_0)\frac{\tau_1}{1+(\omega_N\tau_1)^2}, \quad (3)$$

$$J(0.87\omega_H) = \frac{2}{5}a_0\frac{\tau_0}{1+(0.87\omega_H\tau_0)^2} + \frac{2}{5}(1-a_0)\frac{\tau_1}{1+(0.87\omega_H\tau_1)^2}. \quad (4)$$

The temperature dependence of τ_0 was treated as

$$\tau_0(T) = \frac{\eta}{T}\frac{298\ \mathrm{K}}{\eta(298\ \mathrm{K})}\tau_0(298\ \mathrm{K}), \quad (5)$$

where η is viscosity of pure water at given temperature, and τ_1 was considered to be temperature-independent. The temperature dependence of a_0 was modeled as (Mandel et al., 1996)

$$1 - \sqrt{a_0} = A + \frac{3}{2}\frac{T}{T^*}, \quad (6)$$

where A is an empirical intercept of the linear dependence and T^* is the characteristic temperature defining the force constant of an axially symmetric parabolic potential $E(\theta) = RT^*\theta^2$. The individual models were defined by selection of equations used (Equations 2–4 or Equations 3–4) and of the fit parameters. Table 1 lists the models examined in this study. The model nomenclature introduced in Table 1 is derived from the nomenclature by Mandel et al. (1995). Letters a and b distinguish whether the temperature dependence of a_0 was taken into account, prime indicates that τ_0 was fitted individually for each residue (Schurr et al., 1994), and circle indicates that only Equations 3 and 4 were used for the fit. The parameters not fitted in the individual models were set to zero with the exception of τ_0 that was set to the average of τ_0 values determined in previous fits. Therefore, models marked with prime had to be examined first in order to provide the τ_0 values for the remaining models.

Translational diffusion coefficients D were measured using PFGLED pulse sequence (Waldeck et al., 1997) with WATERGATE water suppression (Piotto et al., 1992) (omitted for measurements of water self-diffusion). Only the samples of 0.5 mM and 1.8 mM

Table 1. Motional parameters obtained by fitting $J(\omega)$ to various mathematical models

Model	Used $J(\omega)$	Fit parameters
1a	$J(0)$, $J(\omega_N)$, $J(0.87\omega_H)$	a_0
2a	$J(0)$, $J(\omega_N)$, $J(0.87\omega_H)$	a_0, τ_1
1b	$J(0)$, $J(\omega_N)$, $J(0.87\omega_H)$	A, $1/T^*$
2b	$J(0)$, $J(\omega_N)$, $J(0.87\omega_H)$	A, $1/T^*$, τ_1
1a′	$J(0)$, $J(\omega_N)$, $J(0.87\omega_H)$	τ_0, a_0
2a′	$J(0)$, $J(\omega_N)$, $J(0.87\omega_H)$	τ_0, a_0, τ_1
1b′	$J(0)$, $J(\omega_N)$, $J(0.87\omega_H)$	τ_0, A, $1/T^*$
2b′	$J(0)$, $J(\omega_N)$, $J(0.87\omega_H)$	τ_0, A, $1/T^*$, τ_1
1a°	$J(\omega_N)$, $J(0.87\omega_H)$	a_0
2a°	$J(\omega_N)$, $J(0.87\omega_H)$	a_0, τ_1
1b°	$J(\omega_N)$, $J(0.87\omega_H)$	A, $1/T^*$
2b°	$J(\omega_N)$, $J(0.87\omega_H)$	A, $1/T^*$, τ_1
3a	$J(0)$, $J(\omega_N)$, $J(0.87\omega_H)$	a_0, A_{ex}, E_{ex}
4a	$J(0)$, $J(\omega_N)$, $J(0.87\omega_H)$	a_0, A_{ex}, E_{ex}, τ_1

free MUP-I were used as the presence of pheromone obscured the most intense peaks of protein in ^{1}H spectra. The pulsed-field gradients were calibrated with a Teflon phantom of known length. The overall rotational correlation time τ_c was determined using Equation 7 (Korzhnev et al., 2001)

$$\tau_c = \left(\frac{k_B T}{\pi\eta}\right)^2 \frac{1}{2D^3}. \quad (7)$$

Viscosity η was estimated from measured selfdiffusion coefficients of water.

Program HYDRONMR (Bernadó et al., 2002) was used to calculate hydrodynamic behaviour of MUP-I. The PDB entry 1IO6 and optimized atomic element radius of 0.30 nm (Bernadó et al., 2002) were used in the calculations.

Results

The relaxation parameters (T_1, T_2 and NOE) were obtained for free and pheromone-bound MUP-I at 283, 288, 293, 298, 303 and 308 K at the magnetic field of 14.1 T (600 MHz). The data were complemented with the relaxation parameters measured at 291, 297, and 302 K at the magnetic field of 11.75 T (500 MHz). The temperature control was checked by monitoring chemical shift changes of selected peaks. No sample overheating was observed as a result of applying radiofrequency pulses. The inspection of chemical shifts showed that the temperature deviated from the expected value during measurements with the free protein at 293 K and 14.1 T. The values of $J(\omega)$ measured at these conditions were also inconsistent with the rest of the data and therefore excluded from further analysis. Data potentially affected by (partial) spectral overlaps were also excluded from the analysis. Intensity of some peaks was substantially lower than the average, resulting in a large experimental error of the measured relaxation data. Five residues of the pheromone-MUP-I complex and eight residues of the free protein were excluded from analysis for this reason. These residues were mostly found in regions 41–43 and 152–160. The observed decrease in signal intensity may reflect increased dynamics and/or solvent accessibility of these backbone amides.

Initially, the relaxation data at each field strength and temperature were analyzed using one of the standard five mathematical models of the (extended) Lipari–Szabo formalism (Lipari and Szabo, 1982a, b; Clore et al., 1990). However, the χ^2 and F-statistical analyses, used for selection of mathematical model in Modelfree software (Mandel et al., 1995), depend on the conditions that influence the experimental error of the relaxation data. As a consequence, comparing results between different temperatures, between the free and bound forms, and between the current and previous data sets is difficult. This is a common problem in the comparison of multiple relaxation data sets for different forms of the same protein (Seewald et al., 2000; K. Mayer et al., manuscript submitted to *Nat. Struct. Biol.*). Therefore, we chose to analyze all the data using the reduced spectral density approach, then to determine the model-free parameters most globally consistent with the reduced spectral densities.

Use of the reduced spectral density mapping has the advantage that the values of spectral density function J at the appropriate frequencies are given as linear combinations of the measured relaxation rates and can be obtained without non-linear data fitting. The only assumption required for reduced spectral density mapping is that the values of spectral density function at frequencies $\omega_H - \omega_N$, ω_H, and $\omega_H + \omega_N$ are almost identical and can be replaced with a single average value $J(0.87\omega_H)$ (Farrow et al., 1995b). Graphical analysis of the spectral density function thus gives an unbiased qualitative picture of the motions. In addition, values of J can be further analyzed in a manner similar to the model-free approach, at the price of loosing generality of the description.

Reduced spectral density mapping

The values of $J(0)$, $J(\omega_N)$, and $J(0.87\omega_H)$, determined as described in the Materials and methods section, are plotted in Figure 1 as a function of the amino-acid sequence. The values of $J(0)$ (Figure 1C) are relatively stable along the sequence, with the exception of a drop at the flexible C-terminus and several elevated values suggesting slow conformational exchange, most notably for residue 62. The temperature dependence of $J(0)$ is mostly given by the dependence of the overall tumbling on the viscosity-to-temperature ratio (η/T) for rigid residues. Therefore, the effect of temperature can be compensated for by multiplying $J(0)$ with $T\eta_{ref}/\eta T_{ref}$, where T_{ref} is a chosen reference temperature (298 K in this study) and η_{ref} is viscosity at this temperature. Assuming that the protein concentration affects only the parameter D_0 in the empirical formula describing the temperature-dependent self-diffusion coefficient of water $D(H_2O) = D_0(T/T_S - 1)^\gamma$ ($T_S = 215$ K, $\gamma = 2.06$; Holz et al., 2000), ratios of viscosities tabulated for pure water can be used. The plot of the temperature-corrected $J(0, 298\ K)$ (Figure 1D) facilitates identification of deviations indicating conformational motions.

The sequence and temperature dependence of $J(0.87\omega_H)$ (Figure 1A) mirrors the course of $J(0)$. In addition to the large increase of $J(0.87\omega_H)$ in the C-terminal regions, slightly increased $J(0.87\omega_H)$ was observed in certain regions of the sequence, most clearly for residues 60–65, 74–77, and 110–114.

The values of $J(\omega_N)$ (Figure 1B) exhibit an intermediate pattern between $J(0)$ and $J(0.87\omega_H)$. Deviations from average values are negligible along the sequence. The temperature dependence of $J(\omega_N)$ is close to that of $J(0.87\omega_H)$ with the exception of the C-terminus, where residue 162 exhibits the reverse dependence (resembling $J(0)$) and residue 160 corresponds to an isosbestic point.

Graphical analysis of spectral densities

The values of spectral density functions available at three frequencies can be visualized as points in a 3D space of dimensions $J(0)$, $J(\omega_N)$, and $J(0.87\omega_H)$. The possibilities of analyzing the spectral density correlation graphs follow from the following considerations. Assuming that the dynamics of the studied N–H groups can be described by m independent motional modes, characterized by correlation times τ_j, the spectral density function is given as a sum of m Lorentzians (Ishima and Nagayama, 1995):

$$J(\omega) = \frac{2}{5}\sum_{j=0}^{m-1} a_j \frac{\tau_j}{1 + (\omega\tau_j)^2}, \tag{8}$$

where the coefficients a_j represent relative contribution of individual motional modes and therefore

$$\sum_{j=0}^{m-1} a_j = 1. \tag{9}$$

If the dynamics is limited to a single motion, Equation 8 is reduced to a single Lorentzian. In such case, $J(0) = 0.4\tau$, and the correlation between $J(0)$ and the spectral density at frequency ω is given simply as

$$J(\omega) = \frac{J(0)}{1 + 6.25(\omega J(0))^2}. \tag{10}$$

Figure 2A illustrates the basic ideas of the analysis for the $J(0)$ *vs.* $J(\omega_N)$ correlation. Solid curves in Figure 2 are defined by Equation 10 and therefore represent all possible positions of points corresponding to the case of dynamics reduced to a single motion, and are effectivelly plots of J as a function of τ. Point P represents an N–H bond motion completely dominated by the overall isotropic tumbling. The $J(0)$-coordinate of P is thus equal to two-fifths of the overall rotational correlation time. Similarly, point Q represents an N–H bond completely dominated by a fast internal motion. Realistic values of measured spectral density functions describing the picosecond-to-nanosecond dynamics should be found between these two limits, as represented by point R. The situation can be further complicated by conformational motions on the microsecond-to-millisecond time scale that increase $J(0)$ by a value of $2R_{ex}/(9d^2 + 3c^2)$ (point S), where R_{ex} is the conformation exchange contribution to the relaxation rate constant R_2 (Mandel et al., 1996). The real data provide a large set of points measured for many residues at several temperatures instead of a single point R (or S) shown in Figure 2A. The analysis can focus on the shape of the complete 'cloud' of data points (Approach I), on sets of points obtained for an individual residue at various temperatures (Approach II), on sets of points measured for all residues at a single temperature (Approach III), or on individual points obtained for one residue at one temperature (Approach IV).

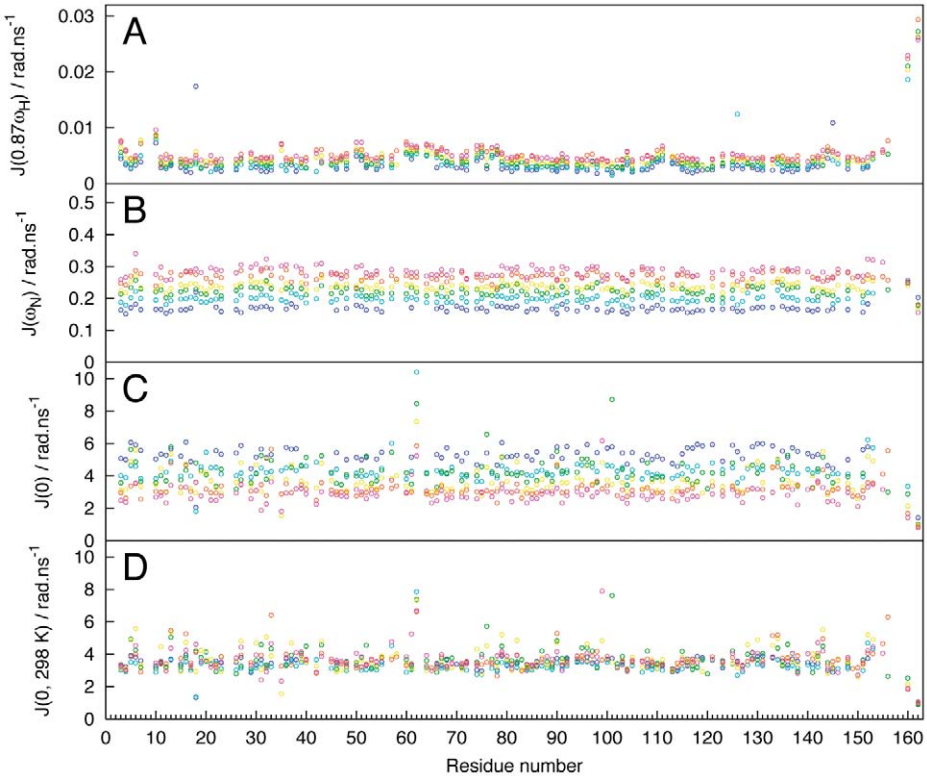

Figure 1. Values of $J(0.87\omega_H)$ (A), $J(\omega_N)$ (B), $J(0)$ (C), and $J(0, 298\ K) = (T\eta_{ref}/\eta T_{ref})J(0)$ for $T_{ref} = 298$ K (D), obtained at 14.1 T for pheromone-bound MUP-I, as functions of the residue number. The following color-coding was used: 283 K, blue; 288 K, cyan; 293 K, green; 298 K, yellow; 303 K, orange; and 308 K, magenta.

The $J(\omega_N)$ vs. $J(0)$ and $J(0.87\omega_H)$ vs. $J(0)$ projections for free MUP-I data measured at 14.1 T are shown in Figures 2B and 2C, respectively. Application of Approach I to all available spectral density values of pheromone-bound MUP-I at 14.1 T (Figures 2A and 2B) show that the correlation graphs exhibit a typical pattern of rigid proteins. Most points are clustered close to the single-Lorentzian limit, described by Equation 10, that is indicative for a rigid particle rotation (Lefèvre et al., 1996; Barthe et al., 1999). Points shifted to the right from the single-Lorentzian limit suggest conformational changes on a μs–ms time scale while few points of high $J(0.87\omega_H)$ and low $J(0)$ correspond to the flexible ends of the molecule (see below). Very similar plots were obtained for the free protein at 14.1 T and for both samples at 11.75 T (not shown).

A good qualitative picture of site-specific dynamics can be obtained by constructing plots introduced in Figure 2 for individual residues (Approach II). Based on such graphs, amino acids can be classified into three basic categories.

The first category can be described as flexible residues with little restriction of the backbone N–H vector motions. Such residues are manifested by low $J(0)$ and high $J(0.87\omega_H)$. Only residues 160 and 162 (Figure 2D) can be classified in this way (spectral peaks of C-terminal residues 159 and 161 overlap with each other and with peaks of residues 132 and 147; the spectral peak of residue 2 overlaps with those of residues 34 and 49).

The second category represents largely rigid residues exhibiting no obvious sign of a slow conformational exchange. Most amino acids of both free and ligand-bound MUP-I belonged to this category. Gly 111 as an example is presented in Figure 2E. The points of the free protein lie closer to the single-Lorentzian limit in most cases, indicating higher rigidity of free MUP-I compared to the protein-pheromone complex, as observed in our previous study (Žídek et al., 1999a). In order to monitor the flexibility increase in a qualitative but unbiased manner, the rigidity change index (RCI) was introduced (see Materials and methods). Values of RCI can vary from

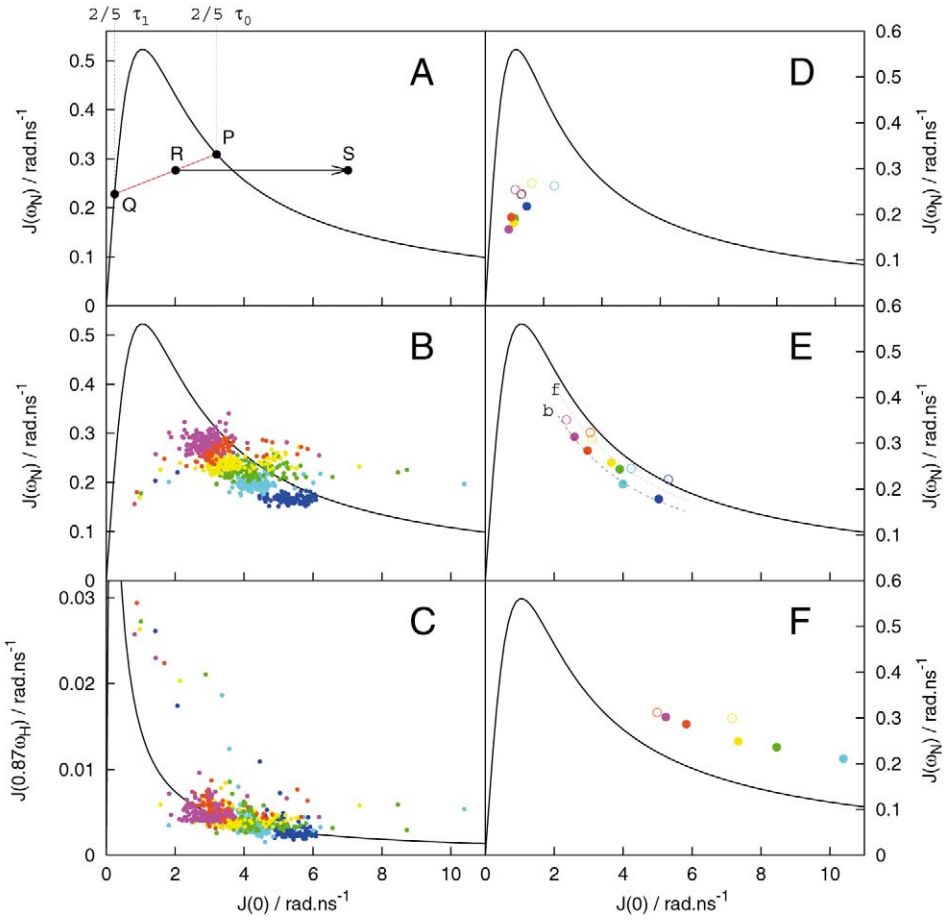

Figure 2. Graphical analysis of spectral density values. (A) illustrates the description of graphical analysis discussed in the text. All available values of $J(\omega_N)$ and $J(0.87\omega_H)$ as functions of $J(0)$ for the pheromone-bound MUP-I at 14.1 T are shown in (B) and (C), respectively. (D) to (F) show values of $J(\omega_N)$ vs. $J(0)$ for selected residues of the pheromone-bound (filled circles) and free (open circles) MUP-I at 14.1 T (Glu 162, (D); Gly 111, (E); and Glu 62, (F)). Solid line represents the limit case of J given by a single Lorentzian (Equation 10). Curves *b* and *f*, used in the RCI method (see Materials and methods), were provided by mathematical model 2a′. The RCI value for Gly 111 was −1.0. The same color-coding was used as described for Figure 1.

+1 (all data points indicate rigidity increase upon pheromone binding) to −1 (all data points indicate rigidity decrease upon pheromone binding). Forty percent residues exhibited RCI lower than −0.5 while only 7% residues exhibited RCI higher than 0.5. It should be noted that although the curves *b* and *f* displayed in Figure 2E were obtained using model 2a′ (see below), use of arbitrary curves that match the distribution of data points reasonably well is possible. Therefore, the RCI method is independent of selection of a mathematical model.

The third category represents residues experiencing conformational exchange on μs–ms time scale. The conformational exchange results in increasing values of $J(0)$ without affecting $J(\omega_N)$ or $J(0.87\omega_H)$. The largest effect of the conformational exchange was observed for residue 62 (Figure 2F). Small exchange contributions can be obscured by the increased flexibility on the ps–ns time scale. It is therefore desirable to take into account other indications of conformational exchange than the elevated $J(0)$ values. Here, the $J(0)$ values obtained at 14.1 and 11.75 T were compared because $J(0)$ is independent of the field strength, except for the exchange term. Also deviations of the temperature-corrected $J(0, 298\ \mathrm{K})$ values were inspected as potential signs of the conformational exchange. Although the data did not always allow a clear distinction between the second and third category, the following residues were classified as exhibiting signs of conformational exchange in the

pheromone-bound MUP-I: 5, 6, 13, 16, 27, 33, 43, 57, 62, 79, 90, 95, 99, 133, 134, 143, 152 and 153. Similar results were obtained for the free protein, with the exception of residues 95 and 133. On the other hand, residue 37 exhibited signs of the conformational exchange in the free protein. In addition, residues 20 and 58, partially overlapped in the spectrum of the pheromone-bound MUP-I, exhibited conformational exchange in the free protein.

Analysis of all residues at individual temperatures (Approach III) can be used to extract information about the global tumbling of the protein. In the case of flexible proteins, data points are evenly distributed between the rigid and flexible limit of the correlation graph (points P and Q in Figure 2A, respectively). The data then can be fitted to a linear function of $J(0)$ (Lefèvre et al., 1996) (red line in Figure 2A). The $J(0)$ coordinates of the intercepts of the obtained line with the single-Lorentzian limit curve then provide global external (point P) and internal (point Q) correlation times (Lefèvre et al., 1996; Barthe et al., 1999). The lack of flexible residues in MUP-I prohibited exact determination of the global internal correlation times (point Q). However, good estimates of the second intersections (point P), providing the overall tumbling correlation times τ_c, could be obtained in spite of the poor definition of the slopes of the mentioned linear correlations. Temperature dependence of the estimated external correlation times, and of most data points in general, essentially reflects variation of the viscosity-to-temperature ratio (η/T) as is discussed below in more detail.

Analysis of individual data points (Approach IV) represents a graphical form of the Lipari–Szabo analysis. Although such approach potentially provides the motional parameters for each temperature, it was not used in this study. Instead, the motional parameters were obtained by a more precise simultaneous fitting of spectral density values to mathematical models including the temperature dependence of the fitted parameters, as described in the following section.

Model-free motional parameters

In order to obtain a more physically intuitive description of the backbone dynamics, the spectral density values for each N–H group in each form of MUP-I were interpreted using mathematical models similar to the original and extended forms of Lipari–Szabo formalism (Lipari and Szabo, 1982a, b; Clore et al., 1990). The relationships between the spectral densities and the are given by Equations 2 to 4 (see Materials and methods). Using the measured values of $J(0)$, $J(\omega_N)$ and $J(0.87\omega_H)$ for an individual residue at a specific temperature, one can determine up to three model-free dynamics parameters in Equations 2–4. However, if the temperature dependence of these parameters is known, one can simultaneously fit the spectral density values determined at multiple temperatures, yielding a larger number and/or higher reliability of the obtained parameters. In this study multiple temperatures were utilized to examine the temperature dependence of the parameters. The overall rotational correlation time should follow the Stokes–Einstein equation with clearly defined temperature dependence. Therefore its values can be used to check the consistency of the experimental data. The internal motional parameters vary with temperature in a less predictable manner. Nevertheless, their temperature dependence should fall into reasonable physical limits. Strong deviations indicate erroneous data.

The mathematical models were derived from the first two terms of the general multi-Lorentzian expansions of J (Ishima and Nagayama, 1995) as described in Materials and methods (Equations 2–4). In such approximation, the coefficient a_0 and correlation times τ_0 and τ_1 directly correspond to the generalized order parameter and global and effective internal correlation times of Lipari and Szabo (1982a), respectively. It should be noted that the mathematical models also introduce the question of the appropriate model selections, as it is known from the Lipari–Szabo approach. The obtained motional parameters are no longer unbiased as were the qualitative results of the graphical analysis described above. The issue of model selection is not addressed in this study. Our goal was only to present mathematitcal models providing motional parameters by fitting temperature-dependent spectral density values. Detailed discussions of the statistical procedures employed to select the most appropriate model can be found in literature (for example, see d'Auvergne and Gooley, 2003).

As the molecule of MUP-I is nearly spherical and rotates almost isotropicly, single correlation time is sufficient to describe its rotational diffusion within an error of ±5% (see below for discussion of anisotropic effects). Therefore, the interpretation of τ_0 as the correlation time of the overall isotropic tumbling τ_c is well justified. The overall rotational correlation time was assumed to be proportional to η/T, as expected from the Stokes–Einstein relationship (Seewald et al., 2000).

The second correlation time, $\tau_1 = (\tau_0^{-1} + \tau_i^{-1})^{-1}$, can be approximated by the internal correlation time τ_i for fast internal motions when $\tau_0 \gg \tau_i$. The energy barriers of the fast motions are usually too low to allow the temperature dependence of τ_i to be estimated (Mandel et al., 1996). Therefore, τ_1 was treated as temperature-independent in the fits.

The temperature dependence of the parameter a_0 (interpreted as the generalized order parameter) is related to the heat capacity C_p of the N–H bond motions. A simple model describing the temperature dependence of a_0 by Equation 6 was proposed by Mandel et al. (1996). A very small slope of the linear temperature dependence assumed by Equation 6 is typical for rigid residues while somewhat larger slope is usually observed for flexible residues (Mandel et al., 1996; Bertini et al., 2000). Two sets of fits were used in this study, either defining a_0 as a single temperature-independent parameter or using A and $1/T^*$ as the fitted parameters. Note that Equation 6 imposes the additional assumption of an axially-symmetric parabolic potential, somewhat limiting the 'model-free' nature of this approach.

For each of the data analyses described below, we performed global fits of the model-free dynamics parameters to the spectral density values (three or two times the number of temperatures) for a particular residue at a specific field strength, as described in Table 1.

For the models using fixed τ_0, it was necessary to obtain an estimate of the overall rotational correlation time. This was calculated as an average of the fitted τ_0 values from model 2a′, including only rigid residues that exhibited no sign of conformational exchange (second category in the classification described above), that had slowly exchanging amide protons (negligible exchange observed after 24 h, data not shown), and that had relaxation data measured at more than two temperatures. The calculated average values were 9.41 ± 0.36 ns for pheromone-bound and 9.38 ± 0.45 ns (expressed for 298 K at 14.1 T). Somewhat higher averages (9.94 ± 0.36 ns and 10.22 ± 0.44 ns, respectively) were obtained at 11.75 T. Similar values were reported in the previous study (9.8 ns and 9.7 ns , respectively, recalculated for 298 K, Žídek et al., 1999a). The obtained values of τ_0 were close to the values of the overall rotational correlation time calculated by the conventional model-free method for model selection 2 (Mandel et al., 1995) (9.9 ± 0.9 ns for pheromone-bound and 9.2 ± 0.5 ns for free MUP-I at 14.1 T). Average values of the translational diffusion coefficient D, measured at 298, 303, and 308 K, provided estimates of τ_c at 298 K equal to 9.6 ± 0.8 ns for 1.8 mM MUP-I and 8.9 ± 0.4 ns for 0.5 mM MUP-I. Although the obtained values nicely fit the other estimates of τ_c, the results should be interpreted carefully as τ_c is proportional to D^{-3} and small systematic errors in determination of D would have large effect on the resulting τ_c.

Hydrodynamic calculations using the program HYDRONMR revealed an important source of the variability of the determined τ_0 values. Figure 3 shows comparison of τ_0 fitted to the spectral density values at 14.1 T and the harmonic mean values of rotational correlation time calculated using program HYDRONMR. The changes of the apparent correlation time along the sequence, as predicted by the hydrodynamic calculations, nicely fit the actual deviations of the data obtained from the relaxation measurements. Note that the only adjustable parameter in the hydrodynamic calculations is the apparent atomic radius. The optimized value used in this study, 0.30 nm, is in the typical range of 0.28 to 0.38 nm (Bernadó et al., 2002). The obtained general anisotropic rotational tensor was characterized by $D_\parallel/D_\perp = 2D_{zz}/(D_{xx} + D_{yy}) = 1.139$ and asymmetry $(D_{xx} - D_{yy})/D_{zz} = 0.030$, corresponding to the following five correlation times: 9.86, 9.70, 9.54, 9.01 and 9.00 ns (harmonic mean value 9.41 ns). The distribution of τ_0 calculated from the previously reported (Žídek et al., 1999a) relaxation parameters (data not shown) did not exhibit the obvious correlation with the results of the hydrodynamic correlation, as shown for the current data.

Figure 4 presents an example of the internal motional parameters obtained by fitting spectral density values. Comparison of some parameteres obtained using different models is shown in Figure 5. Note that the values determined for residues exhibiting signs of the slow conformational exchange are included in Figure 4 (open symbols) although these residues are not well described by these particular models.

The absolute values of a_0 determined in this study are higher than the previously reported values (Žídek et al., 1999a). The difference in a_0 reflects the fact that the measured relaxation rates were higher in this study than in the previous work. Although the source of the systematic difference between these two studies remains unclear, one possibility is the bias introduced by the exponential fitting errors. Such bias of curve fitting methods has been recently discussed by Viles and coworkers (Viles et al., 2001). The issue of the systematic errors in determining relaxation para-

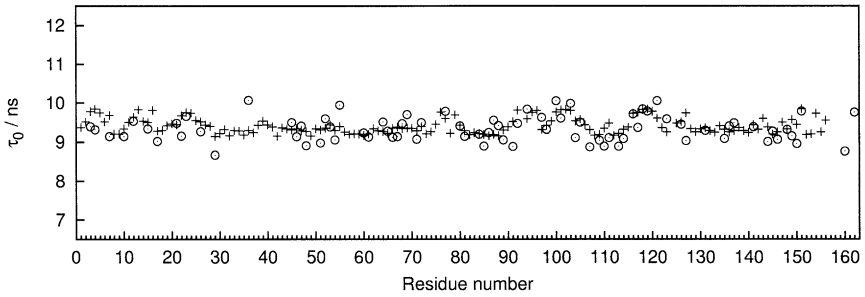

Figure 3. Comparison of harmonic mean roational correlation times obtained from hydrodynamic calculations (crosses) and τ_0 calculated using model 2a′ (1a′ in cases when $\tau_1 < 0$ was obtained) for pheromone-bound MUP-I (circles) at 14.1 T.

meters is important but it exceeds the scope of this paper, dedicated to the temperature-dependent spectral density analysis. A study focused on the origin of errors and on improving reproducibility of relaxation measurements is currently in progress in our laboratory.

Comparison of the a_0 values determined for free and pheromone-bound MUP-I showed that a_0 decreased for most residues upon pheromone binding. This finding is in a good agreement with the results of the qualitative graphical analysis using RCI (see above) and with the previously reported data (Žídek et al., 1999a, Figure 4). The previously reported increase in flexibility upon pheromone binding was thus reproduced in spite of the mentioned systematic difference between the absolute values of a_0.

Values of the characteristic temperature T^* (see Figure 5) were larger than 450 K for most residues, with the exception of terminal Glu 162 ($T^* = 190$ K). These values are in a good agreement with results of Mandel and coworkers (Mandel et al., 1996) who reported values of T^* in a range from 170 K (flexible residues) to 1000 K (rigid residues) for ribonuclease H. Similar values were also recently published by Spyracopoulos and coworkers, who monitored dynamics of the human cardiac troponin C regulatory domain at eight temperatures (Spyracopoulos et al., 2001).

The parameters A_{ex} and E_{ex} were obtained with a too large uncertainty to allow any conclusions for most residues. The noteworthy exception was residue 62 that exhibited the largest exchange term with well-defined temperature dependence ($E_{ex} = 34 \pm 11$ kJ mol^{-1} for model 3a). In spite of the uncertainty in the exchange term, the obtained τ_1 profiles were similar and a_0 values almost identical to the output of the corresponding exchange-free models.

As only $J(0)$ is affected by the slow conformational exchange, fits independent of this influence can be obtained using only the values $J(\omega_N)$ and $J(0.87\omega_H)$. The penalty paid for this advantage is a smaller number of parameters that can be fit. The estimated parameters a_0 and τ_1 (together with the used value of τ_0) can be used to simulate $J(0)$ according to Equation 2. The difference between the simulated and experimental values of $J(0)$ then provides the values of the exchange term. The exchange contribution determined by this approach (Figure 6) corresponded very well to the qualitative classification of residues described above. In accordance with the results discussed above, the largest contribution of the conformational exchange was observed for residue 62. In this case, the relation included in Equation 2 could be applied and parameters A_{ex} and E_{ex} were determined. For the pheromone-bound sample measured at 14.1 T, where the best experimental data were available, the determined values were $E_{ex} = 33.5 \pm 2.5$ kJ mol^{-1}, $A_{ex} = -12.2 \pm 1.0$ (model 2a°) and $E_{ex} = 31.7 \pm 2.5$ kJ mol^{-1}, $A_{ex} = -11.5 \pm 1.0$ (model 2b°). About twofold higher E_{ex} values were obtained for the free protein. However, data measured at only three temperatures were available for free MUP-I, so the latter results must be interpreted with caution. In any case, the determined values are virtually identical to those obtained when fitting $J(0)$, $J(\omega_N)$, and $J(0.87\omega_H)$ simultaneously.

Discussion

Temperature-dependent NMR relaxation of the backbone amide bond was analyzed in order to investigate the interesting dynamic behavior of the complex of MUP-I with 2-*sec*-butyl-4,5-dihydrothiazole revealed in our previous study (Žídek et al., 1999a). As the con-

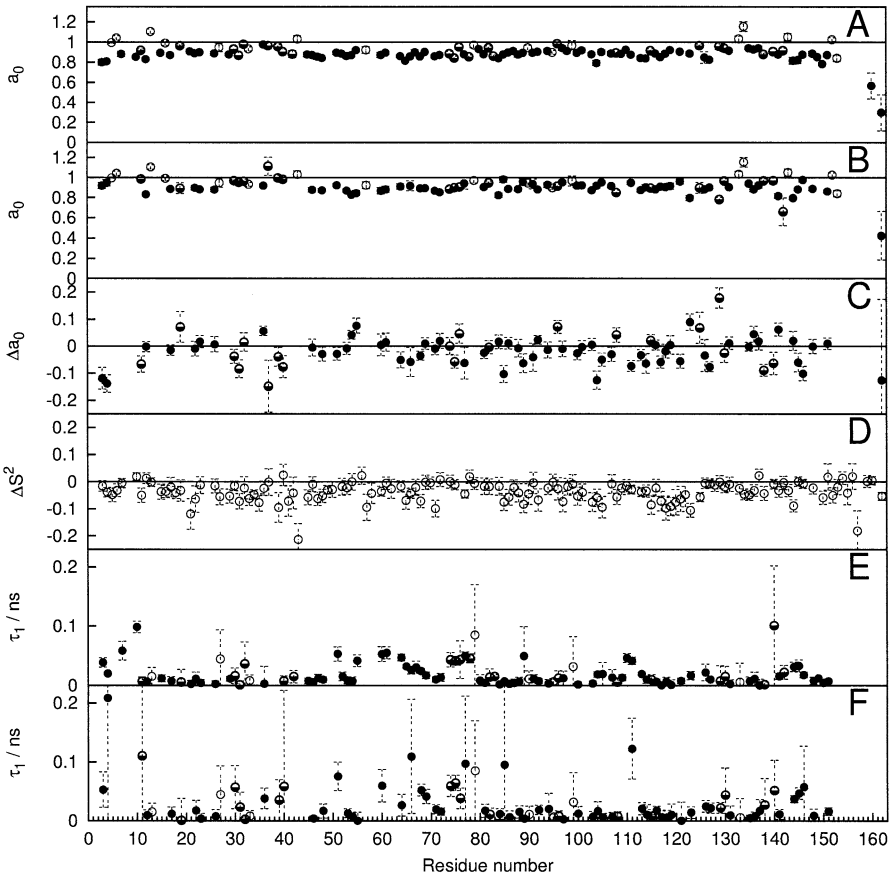

Figure 4. Results of fitting $J(0)$, $J(\omega_N)$, and $J(0.87\omega_H)$, obtained at 14.1 T, to the mathematical models including τ_0, a_0, and τ_1. The motional parameters were obtained using model 2a′ if the fit $\tau_1 > 0$, otherwise model 1a′ was used. Fitted values of a_0 are presented in (A) (pheromone-MUP-I complex), (B) (free MUP-I), and (C) (change of a_0 upon pheromone binding). (E) and (F) show fitted values of short τ_1 for pheromone-bound and free MUP-I, respectively. Filled circles represent residues exhibiting no sign of slow conformational exchange, open circles represent residues undergoing slow conformational exchange, and half-filled circles represent cases when the slow exchange was not clearly excluded or identified. The error bars correspond to the standard deviation of the multi-temperature fit. For the sake of comparison, previously reported changes of the Lipari–Szabo generalized order parameter S^2 are shown in (D) (standard deviations calculated by Monte-Carlo simulations are shown as error bars). Note that values in (D) are presented for all residues, including those that exhibited slow conformational exchange in this study.

clusions of the previous article were based on rather subtle changes in the order parameter, higher magnetic field, 3.6-fold higher sample concentration, and repeated measurements at various temperatures were employed in this study.

The data were analyzed according to the reduced spectral density mapping approach, yielding parameters that are independent of the mathematical form of the correlation function. Subsequently, the spectral density values were interpreted using a novel global analysis of the multiple-temperature data to yield consensus values comparable to the Lipari–Szabo model-free parameters. The estimated values of the overall rotational correlation time exhibited the expected temperature dependence, following the Stokes–Einstein law. Small sequence-dependent deviations of the overall rotational correlation time from its average value correlated well with the anisotropic behaviour predicted by hydrodynamic calculations (Figure 3).

Regardless of the level of sophistication, all models showed qualitatively (and in many cases also quantitatively) identical picture of the molecular motions in MUP-I. It should be noted that low experimental errors allowed us to obtain reasonable fits using only $J(\omega_N)$, and $J(0.87\omega_H)$ so that the results were not affected by the slow conformational exchange.

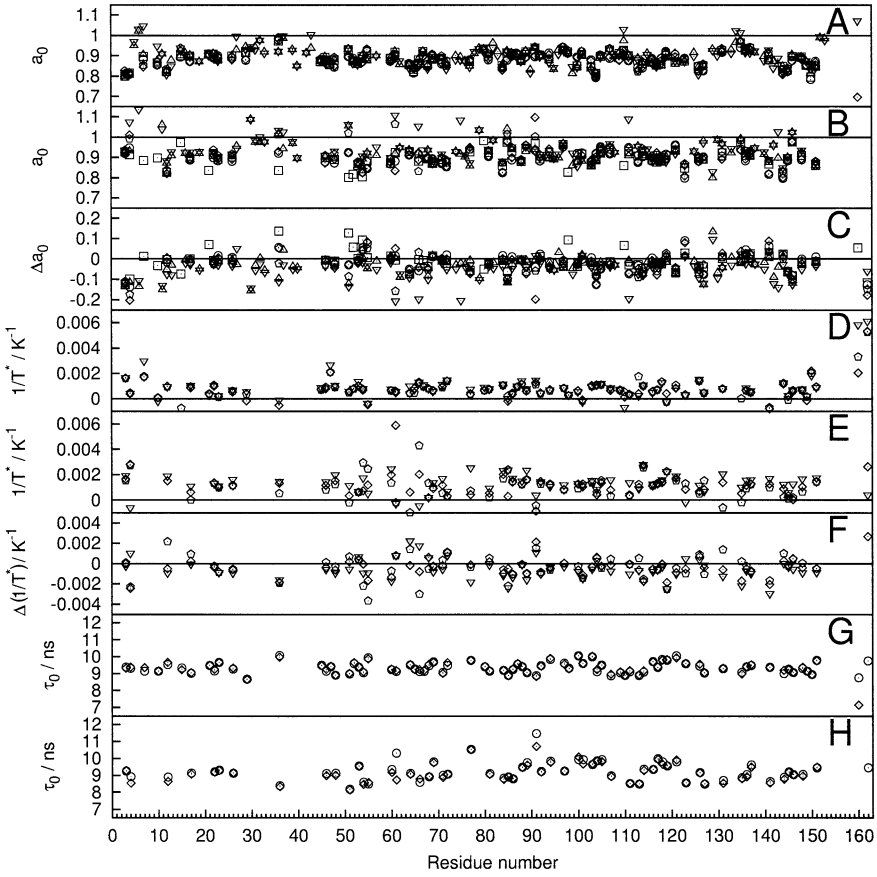

Figure 5. Comparison of a_0 ((A)–(C)), $1/T^*$ ((D)–(F)), and τ_0 ((G) and (H)) obtained from data acquired at 14.1 T using the following motional models: 2a′ (1a′), circles; 2b′ (1b′), diamonds; 2a (1a), squares; 2b (1b), pentagons; 2a° (1a°), triangles pointing up; and 2b° (1b°), triangles pointing down. Results of the models in parentheses are presented if $\tau_1 < 0$ was obtained for the more general models. Results for pheromone-bound MUP-I are presented in (A), (D) and (G), results for free MUP-I are presented in (B), (E) and (H), and changes of a_0 and $1/T^*$ upon pheromone binding is shown in (C) and (F), respectively.

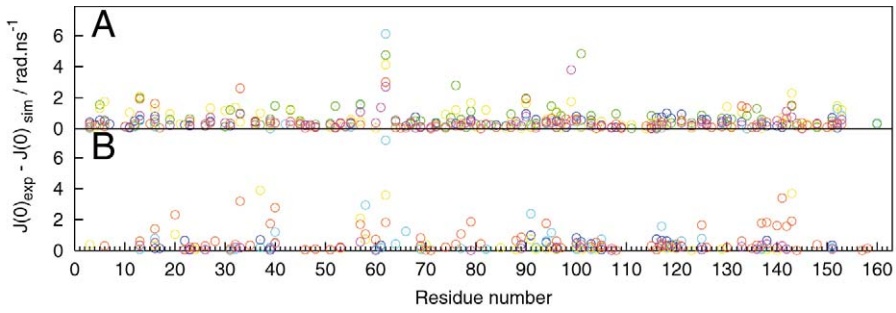

Figure 6. The exchange contribution to $J(0)$ calculated as a difference between the experimental value and the simulated value, calculated from parameters obtained using model 2a° (or 1a°, when $\tau_1 < 0$ was obtained using model 2a°). Data for pheromone-bound (A) and free (B) MUP-I, measured at 14.1 T, are color-coded as described in Figure 2.

Fast internal motions of MUP-I

The reduced spectral density mapping showed that amides of almost all MUP-I residues are rigid in the both free and pheromone-bound form (Figure 2). This finding corresponds well to the compact structure of the MUP-I molecule, dominated by a single β-barrel (Figure 7). The interior of the β-barrel forms a binding site able to accommodate a variety of ligands without changing the overall shape of the molecule. The sequence-specific plots of $J(\omega)$ revealed that only two amino acids represent the category of highly flexible residues on the fast time scale. Both of them are located at the C-terminus (Ala 160 and the terminal Glu 162). Although data for some residues are missing, the results clearly show that the backbone is relatively rigid between residues 3 and 158. Nevertheless, slightly higher values of $J(0.87\omega_H)$ indicate certain enhancement of rapid motions in several regions of the molecule (Figure 1). The same regions also displayed slightly lower than typical values of the fitted a_0 parameters (Figures 4 and 5). In all cases, the increased flexibility was observed in connections between secondary structure elements or in terminal regions of the corresponding secondary structures. The most significant increase of flexibility was observed for connections between long β-strands C and D, G and H, the region between the long α helix and strand I, and for the region preceding the C-terminal 3_{10}-helix. Note that the mobile portions of strands C, D and H are only partially involved in a hydrogen-bond network. It should be noted that these conclusions regarding fast internal motions were also confirmed by fitting only $J(\omega_N)$ and $J(0.87\omega_H)$, implying they are not affected by the slow conformational exchange.

Subtle changes of the fast internal dynamics between the free and bound forms of MUP-I were investigated by comparing the graphs of $J(\omega_N)$ as a function of $J(0)$ (Figure 2E). Most residues experienced higher contributions of the fast internal motions in the pheromone-bound form. Quantitative description of this phenomenon was obtained by fitting the experimental data to several mathematical models. Regardless of the model, increased contribution of the rapid motions, given by the value of $1 - a_0$, were observed upon pheromone binding. Although the absolute values of the fitted a_0 were higher by approximately 0.1 than the previously measured order parameters, the estimated a_0 differences varied with the amino-acid sequence in a reasonable general agreement with the previously published values of the order parameter decrease (Žídek et al., 1999a). Thus, the present study corroborates the previous evidence that pheromone-binding slightly increases the backbone flexibility of MUP-I. Although it is more common to observe decreases in protein dynamics upon ligand-binding, there is an increasing number of cases (Stivers et al., 1996; Arumugam et al., 2003; Fayos et al., 2003) in which flexibility increases in specific regions of a protein, presumably providing an entropic driving force for the binding interaction. Interestingly, one would expect increased flexibility to be associated with low specificity of binding, which is the case for MUP-I (Sharrow et al., 2002).

In addition to supporting the previous conclusion that the backbone flexibility of MUP-I increases slightly upon pheromone-binding, the current temperature-dependent data have the potential to shed light on the contribution of conformational heat capacity to the binding process. Heat capacity C_p is defined as the partial derivative of entropy with respect to the natural logarithm of temperature. In the current study, the backbone motional amplitudes (a_0 values) are related to conformational entropy, subject to the assumptions discussed elsewhere (Stone, 2001). Thus, the temperature-dependence of a_0 represented in our analysis by the characteristic temperature T^*, is related to conformational heat capacity; higher values of $1/T^*$ (lower values of $T*$) correspond to higher capacity values.

Figure 5 shows the values of $1/T^*$ for the free and pheromone-bound forms of MUP-I as well as the difference between the two forms. In most cases the differences between the two forms are very small and within the uncertainty of the measurements. Thus, the data do not provide strong evidence for a change in conformational heat capacity upon ligand-binding. Nevertheless, on average $1/T^*$ decreases slightly upon binding, suggesting the possibility that conformational fluctuations make a negative contribution to the heat capacity of binding. Notably, the overall heat capacity of binding is also large and negative $\Delta C_p = -0.69 \pm 0.04\,\mathrm{J\,mol^{-1}\,K^{-1}}$, although the latter is likely to be dominated by solvation effects rather than conformational fluctuations. Taken together, the previous and current dynamics data suggest theat the backbone conformational entropy of MUP-I at 25–30 °C increases upon binding to the pheromone, but that this entropy increase becomes slightly less dramatic at higher temperatures. This thermodynamic profile is reminiscent of the hydrophobic effect, in which release of ordered water from hydrophobic surfaces is

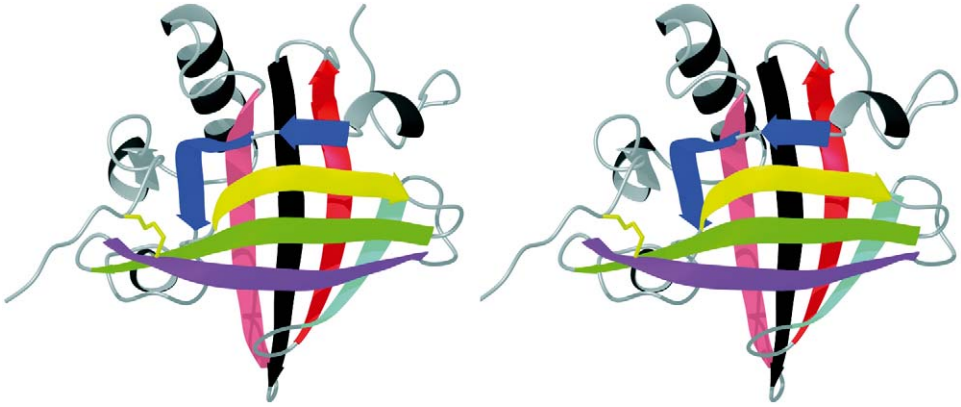

Figure 7. Stereo ribbon diagram of MUP-I (PDB entry 1IO6 with the C-terminal residues added to the model). The β strands are color-coded as follows: A, blue; B, yellow; C, green; D, magenta; E, cyan; F, red; G, black; and H, pink. Short strand I and helical regions are shown in gray. Cystein side-chains forming disulfide bond are indicated with yellow.

associated with increased entropy and decreased heat capacity. We previously speculated that the observed enhancement of backbone flexibility might be coupled to the release of ordered water from the binding cavity. The current observations are consistent with this proposal, althoush it remains to be better established for example by crystallographic or NMR observations of bound water.

Slow internal motions of MUP-I

The information about slow conformational changes, occurring on the μs–ms time scale, was obtained from the $J(0)$ data. Differences between data obtained at 14.1 and 11.75 T, thermal variations of the temperature-corrected $J(0, 298\ \mathrm{K})$ values, and unusually increased $J(0)$ were taken as signs of the slow conformational exchange. Alternatively, motional parameters were obtained by fitting only the exchange-independent $J(\omega_N)$ and $J(0.87\omega_H)$ data and their values were used to simulate $J(0)$. The difference between the simulated and measured $J(0)$ values was taken as the exchange contribution to $J(0)$. Both methods lead to identical selection of approximately 15% residues classified as mobile on the μs–ms time scale. About the same number of residues exhibited weaker indications of exchange at the border of experimental uncertainty (Figure 4). Most of the residues undergoing the slow conformational exchange were located in the unstructured and helical regions of the protein (Figure 8), with the exception of Phe 90, located in the middle of strand F, and of His 57 and Thr 58, located in strand C. Glu 62, located in a β-turn connecting long strands C and D, exhibited extremely high exchange contribution, uncomparable to any other measured residue in MUP-I. Interestingly, this region is covalently bound to the unstructured C-terminus via disulfide bridge between Cys 64 and Cys 157 (Figure 7). No significant differences between the free and pheromone-bound MUP-I were observed. Therefore, we did not pursue a more detailed characterization of exchange rates, e.g. using relaxation dispersion measurements.

Temperature dependence of the exchange contribution was discussed by Mandel and coworkers (Mandel et al., 1996). They showed that the exchange term increases with increasing temperature when the exchange is slower that the CPMG delay, and decreases with increasing temperature when the exchange is faster. If the exchange is sufficiently fast, the exchange term is proportional to the inverse of the exchange rate. The activation energy of the exchange can be then estimated from the Arrhenius plot if the thermal changes of chemical shift are neglected and the free energy is assumed to be close to zero. The exchange contributions were too small to determine reliable values of activation energy for most residues. The only exception was Glu 62 for which the apparent activation energy of 30 kJ mol^{-1} was estimated in the protein-pheromone complex.

Conclusions

NMR relaxation parameters of free and pheromone-bound MUP-I were measured at multiple temperatures and a novel methodology of temperature-dependent reduced spectral density mapping was introduced. Fast

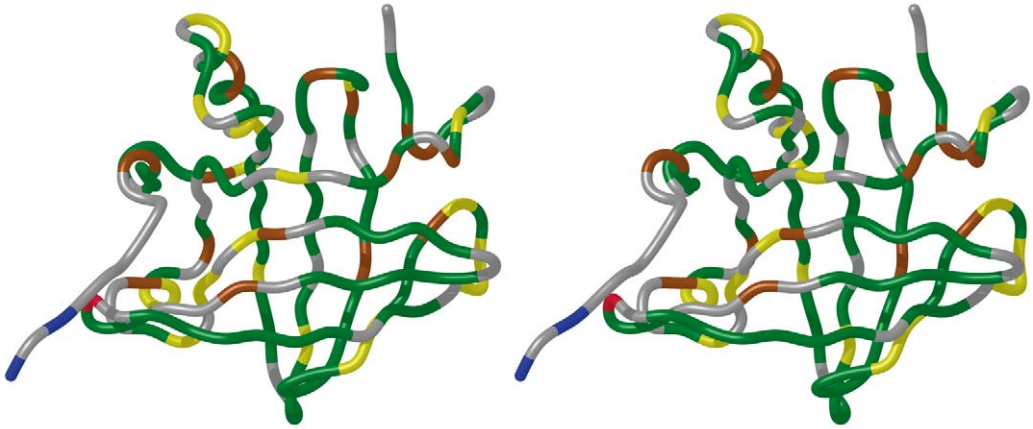

Figure 8. Stereo diagram of motional categories of MUP-I residues. Blue color indicates residues flexible on the fast time scale, green color indicates residues relatively rigid on the fast time scale and showing no signs of slow conformational motions, orange color marks residues exhibiting slow conformational exchange, and yellow color indicates possible signs of slow conformational motions at the border of experimental significance. Glu 62, exhibiting extremely high contribution of the slow conformational exchange, is shown in red.

motions were described qualitatively using a graphical spectral density analysis and quantitatively, yielding motional parameters directly comparable to those obtained by the Lipari–Szabo method. In addition, the spectral density values evaluated at zero frequency provided information about the slow conformational changes. The results showed that the dynamics of the two forms of MUP-I are similar but that there is a subtle increase in fast time scale flexibility in the pheromone-bound form, in an agreement with the previously reported data.

Acknowledgements

The authors thank P. Padrta, J. Chmelík and P. Macek for technical help and R. Fiala for critical reading the manuscript.

References

Arumugam, S., Gao, G.H., Patton, B.L., Semenchenko, V., Brew, K. and Van Doren, S.R. (2003) *J. Mol. Biol.*, **327**, 719–734.

Barthe, P., Chiche, L., Declerck, N., Delsuc, M.A., Lefèvre, J.F., Malliavin, T., Mispelter, J., Stern, M.H., Lhoste, J.M. and Roumestand, C. (1999) *J. Biomol. NMR*, **15**, 271–288.

Bernadó, P., García de la Torre, J. and Pons, M. (2002) *J. Biomol. NMR*, **23**, 139–150.

Bertini, I., Luchinat, C., Niikura, Y. and Presenti, C. (2000) *Proteins*, **41**, 75–85.

Beynon, R. J., Veggerby, C., Payne, C.E., Robertson, D.H.L., Gaskell, S.J., Humphries, R.E. and Hurst, J.L. (2002) *J. Chem. Ecol.*, **28**, 1429–1446.

Böcskei, Z., Groom, C.R., Flower, D.R., Wright, C.E., Phillips, S.E.V., Cavaggioni, A., Findlay, J.B.C. and North, A.C.T. (1992) *Nature*, **360**, 186–188.

Bracken, C., Carr, P.A., Cavanagh, J. and Palmer, A.G. (1999) *J. Mol. Biol.*, **285**, 2133–2146.

Clore, G.M., Szabo, A., Bax, A., Kay, L.E., Driscoll, P.C. and Gronenborn, A.M. (1990) *J. Am. Chem. Soc.*, **112**, 4989–4991.

d'Auvergne, E.J. and Gooley, P.R. (2003) *J. Biomol. NMR*, **25**, 25–39.

Delaglio, F., Grzesiek, S., Vuister, G.W., Zhu, G., Pfeifer, J. and Bax, A. (1995) *J. Biomol. NMR*, **6**, 277–293.

Evenäs, J., Forsén, S., Malmendal, A. and Akke, M. (1999) *J. Mol. Biol.*, **289**, 603–617.

Farrow, N.A., Muhandiram, R., Singer, A.U., Pascal, S.M., Kay, C.M., Gish, G., Shoelson, S.E., Pawson, T., Forman-Kay, J.D. and Kay, L.E. (1994) *Biochemistry*, **33**, 5984–6003.

Farrow, N.A., Zhang, O.W., Forman-Kay, J.D. and Kay, L.E. (1995a) *Biochemistry*, **34**, 868–878.

Farrow, N.A., Zhang, O.W., Szabo, A., Torchia, D.A. and Kay, L.E. (1995b) *J. Biomol. NMR*, **6**, 153–162.

Fayos, R., Melacini, G., Newlon, M.G., Burns, L., Scott, J.D. and Jennings, P.A. (2003) *J. Biol. Chem.*, **278**, 18581–18587.

Flower, D.R. (1996) *Biochem. J.*, **318**, 1–14.

Holz, M., Heil, S.R. and Sacco, A. (2000) *Phys. Chem. Chem. Phys.*, **2**, 4740–4742.

Hurst, J.L., Payne, C.E., Nevison, C.M., Marie, A.D., Humphries, R.E., Robertson, D.H.L., Cavaggioni, A. and Beynon, R.J. (2001) *Nature*, **414**, 631–634.

Idiyatullin, D., Daragan, V.A. and Mayo, K.H. (2003) *J. Magn. Reson.*, **161**, 118–125.

Ishima, R. and Nagayama, K. (1995) *J. Magn. Reson. Ser.*, **B108**, 73–76.

Korzhnev, D.M., Billeter, M., Arseniev, A.S. and Orekhov, V.Y. (2001) *Prog. Nucl. Magn. Reson. Spectosc.*, **38**, 197–266.

Kuser, P.R., Franzoni, L., Ferrari, E., Spisni, A. and Polikarpov, I. (2001) *Acta Crystallogr. Sect. D-Biol. Crystallogr.*, **57**, 1863–1869.

Landry, S.J., Steede, N.K. and Maskos, K. (1997) *Biochemistry*, **36**, 10975–10986.

Lefèvre, J.F., Dayie, K.T., Peng, J.W. and Wagner, G. (1996) *Biochemistry*, **35**, 2674–2686.
Lipari, G. and Szabo, A. (1982a) *J. Am. Chem. Soc.*, **104**, 4546–4559.
Lipari, G. and Szabo, A. (1982b) *J. Am. Chem. Soc.*, **104**, 4559–4570.
Lücke, C., Franzoni, L., Abbate, F., Löhr, F., Ferrari, E., Sorbi, R.T., Rüterjans, H. and Spisni, A. (1999) *Eur. J. Biochem.*, **266**, 1210–1218.
Mandel, A.M., Akke, M. and Palmer, A.G. (1995) *J. Mol. Biol.*, **246**, 144–163.
Mandel, A.M., Akke, M. and Palmer, A.G. (1996) *Biochemistry*, **35**, 16009–16023.
Marie, A.D., Veggerby, C., Robertson, D.H.L., Gaskell, S.J., Hubbard, S.J., Martinsen, L., Hurst, J.L. and Beynon, R.J. (2001) *Protein Sci.*, **10**, 411–417.
Novotny, M.V., Ma, W.D., Wiesler, D. and Žídek, L. (1999) *Proc. Roy. Soc. Lond. Ser. B-Biol. Sci.*, **266**, 2017–2022.
Novotny, M.V., Xie, T.M., Harvey, S., Wiesler, D., Jemiolo, B. and Carmack, M. (1995) *Experientia*, **51**, 738–743.
Peng, J.W. and Wagner, G. (1995) *Biochemistry*, **34**, 16733–16752.
Piotto, M., Saudek, V. and Sklenář, V. (1992) *J. Biomol. NMR*, **2**, 661–665.
Ramboarina, S., Srividya, N., Atkinson, R.A., Morellet, N., Roques, B.P., Lefèvre, J.F., Mély, Y. and Kieffer, B. (2002) *J. Mol. Biol.*, **316**, 611–627.
Schurr, J.M., Babcock, H.P. and Fujimoto, B.S. (1994) *J. Magn. Reson. Ser.*, **B105**, 211–224.
Seewald, M.J., Pichumani, K., Stowell, C., Tibbals, B.V., Regan, L. and Stone, M.J. (2000) *Protein Sci.*, **9**, 1177–1193.
Sharrow, S.D., Novotny, M.V. and Stone, M.J. (2003) *Biochemistry*, **42**, 6302–6309.
Sharrow, S.D., Vaughn, J.L., Žídek, L., Novotny, M.V. and Stone, M.J. (2002) *Protein Sci.*, **11**, 2247–2256.
Spyracopoulos, L., Lavigne, P., Crump, M.P., Gagne, S.M., Kay, C.M. and Sykes, B.D. (2001) *Biochemistry*, **40**, 12541–12551.
Stivers, J.T., Abeygunawardana, C., Mildvan, A.S. and Whitman, C.P. (1996) *Biochemistry*, **35**, 16036–16047.
Stone, M.J. (2001) *Acc. Chem. Res.*, **34**, 379–388.
Timm, D.E., Baker, L.J., Mueller, H., Žídek, L. and Novotny, M.V. (2001) *Protein Sci.*, **10**, 997–1004.
Viles, J.H., Duggan, B.M., Zaborowski, E., Schwarzinger, S., Huntley, J.J.A., Kroon, G.J.A., Dyson, H.J. and Wright, P.E. (2001) *J. Biomol. NMR*, **21**, 1–9.
Waldeck, A.R., Kuchel, P.W., Lennon, A.J. and Chapman, B.E. (1997) *Prog. Nucl. Magn. Reson. Spectosc.*, **30**, 39–68.
Žídek, L., Novotny, M.V. and Stone, M.J. (1999a) *Nat. Struct. Biol.*, **6**, 1118–1121.
Žídek, L., Stone, M.J., Lato, S.M., Pagel, M.D., Miao, Z.S., Ellington, A.D. and Novotny, M.V. (1999b) *Biochemistry*, **38**, 9850–9861.